Sensors and Materials, Vol. 34, No. 9 (2022) 3411–3427
MYU Tokyo

S & M 3049

A Simplified Model for Calculating the Dependence of Ambient Temperature and Relative Humidity on Commercial Metal Oxide Chemiresistive Gas Sensors

Kizhakkumbadan Sukhdev,[1,2*] Peringot Harinarayanan,[2,3]
Ulayil Sajesh Kumar,[3] and Padiillam Baburaj[1]

[1]EEE Department, Government College of Engineering Kannur, Kerala 670563, India
[2]ECE Department, Government Residential Women's Polytechnic College Payyannur, Kerala 670307, India
[3]ECE Department, Government College of Engineering Kannur, Kerala 670563, India

(Received June 27, 2022; accepted August 15, 2022)

Keywords: modeling, tin dioxide, gas sensor, humidity compensation, temperature compensation

The conductance and sensor response of metal oxide chemiresistive gas sensors have a high dependence on ambient temperature and relative humidity. A simple mathematical model for calculating the dependence on ambient conditions for most of the commercially available metal oxide gas sensors is proposed. The model has an exponential relationship to ambient temperature and a linear relationship to relative humidity. Tin dioxide-based commercial metal oxide gas sensors, produced by Zhengzhou Winsen Electronics Technologies Co. Ltd., are considered for analysis. At various relative humidities, the sensor response is extracted from the sensor response vs temperature curves provided in the datasheets of commercial metal oxide gas sensors. Model parameters are evaluated from the extracted sensor response curves. The sensor responses calculated using the model are compared with those extracted from the datasheets. The model predicts the sensor response with a root mean square (RMS) error of less than 5%. We have also observed that the model with the same model parameter fits multiple sensors. The sensors are deployed at various locations on our campus for four months, along with electrochemical sensors having a higher sensitivity for comparison. The resistance in air measured using the sensors studied was within a limit of ±3% of its average after the correction of the effects of humidity and temperature.

1. Introduction

Metal oxide chemiresistor-based commercial gas sensors are very popular owing to their advantages, such as low cost, easy availability, simple interface circuitry, endurance, and a wide range of detectable gases.[1,2] One of the main drawbacks of the metal oxide sensors is their dependence on ambient temperature and relative humidity, which can add a large difference to the gas concentration read by the sensors.[3] The other main drawbacks are poor selectivity and

*Corresponding author: e-mail: sukhdevk1@gmail.com
https://doi.org/10.18494/SAM3995

ISSN 0914-4935
https://myukk.org/

drift over long-term use. In the Zhengzhou Winsen MQ series gas sensors that we have analyzed, tin dioxide is the sensing layer used.

The electrical resistance of the metal oxide chemiresistive gas sensor varies according to the target gas concentration at its detectable range of gas sensing.[1,4] Metal oxides can be of the p-type or n-type even without doping owing to their crystal properties.[5,6] When an n-type metal oxide is placed in air at a particular temperature, oxygen in the atmosphere is physically or chemically adsorbed on the surface of the metal oxide.[1,2,7,8] At a temperature below 70 °C, oxygen (O_{2phy}) is physically adsorbed on the surface and weakly bonded to the metal oxide without any electron exchange. At temperatures around 150 °C, oxygen is adsorbed in molecular forms with or without ionization (O_{2chem} and O_2^-). Ionized oxygen species in atomic forms (O^- and O^{2-}) are present on the surface in a temperature range of 200–400 °C. At a temperature above 400 °C, all the oxygen species other than O^{2-} are negligible on the surface of a typical semiconducting metal oxide. The oxygen, ionosorbed by capturing electrons from the metal oxide surface, reduces the conductivity of the sensing material.[8,9] When a reducing gas is introduced, the chemisorbed oxygen reacts with the gas. This in turn retains the electrons captured by oxygen, thus increasing the conductivity of the surface. In contrast, in the presence of an oxidizing gas, the conductivity of an n-type metal oxide gas sensor is further reduced as compared with that in pure air. This is because the oxidizing gas is adsorbed on the surface and consumes electrons.[4,9,10] Even though all the metal oxide gas sensors have a built-in microheater (to operate the sensor at an optimum temperature), the ambient temperature and relative humidity have a significant effect on the performance of the sensor. This is because the relative humidity and temperature of different gases of our interest in the surroundings play a key role in the physical and chemical processes occurring on the surface of the sensing layer.[11] At lower temperatures, water molecules are chemically adsorbed on the surface, forming OH^-groups. This will change the oxygen adsorption process and hence alter the operation of the sensor. At higher humidities, H_2O is physically adsorbed on the hydroxyl groups, forming multiple layers of water molecules. This will increase the conductivity of the device. In this case, the sensing properties are lost since there are no free electrons generated during the reaction with the reducing gases. When the relative humidity is less than 20%, it is considered dry air. When the relative humidity is above 90%, it is considered near-saturated humidity. The normal range of operation of the MQ series gas sensors is from 33 to 90% relative humidity.

The MQ series sensors we have considered are sensing reducing gases such as CO, H_2, CH_4, liquefied petroleum gas (LPG), and ethanol, and the built-in heater operates the sensor in the range of 200–400 °C. In this range, ionized oxygen species in atomic forms (O^- and O^{2-}) are present. In dry air, reducing gases react with the adsorbed oxygen as follows.[12,13]

$$CO + O_{ads}^{2-} \rightarrow CO_2 + 2e^- \tag{1}$$

$$CO + O_{ads}^{-} \rightarrow CO_2 + e^- \tag{2}$$

In the normal relative humidity range, water is adsorbed as hydroxyl groups (OH_{ads}^-) and the reducing gases react with the OH_{ads}^- ions as follows.[14]

$$CO + OH^{-}_{ads} \rightarrow H^{+}_{ads} + CO_2 + e^{-} \tag{3}$$

At a near-saturated level of humidity, target gases react with water and form compounds, which are not detectable by the gas sensors or do not remain in the atmosphere. Thus, detection is not possible or not necessary.

The crystal structure and composition of the sensing layer play a key role in the sensor response. The grain radius, presence and size of pores, shape of grains, sensing layer thickness, and the type of defect or impurity are other factors that change the sensor response.[5,15,16] Similarly, some surface or bulk impurities are added to improve the sensitivity, selectivity, and other characteristics of the sensor used.[17,18] However, for a commercially available sensor, these factors are fixed. Hence, the model proposed can be independent of such parameters. There are very few approaches to model the humidity and temperature dependences of commercial metal oxide gas sensors. Most of the modeling approaches published by researchers are meant for the sensors that they fabricated. In such models, the morphology and chemical composition play a key role. A generalization of such models is not possible owing to the nonuniformity in the fabrication process, chemical composition, and morphological aspects.[19,20] In the case of commercial sensors, the morphological aspects are generally not disclosed, and hence such a model is not useful for the end user. AI-based models are reported to give a complicated expression for dependence on ambient conditions because even two metal oxide sensors fabricated by the same process may behave very differently depending on the environment of operation or storage.[21,22] This makes the calibration and training very difficult.[23] In other words, we may need to do the modeling for each sensor whenever it is first used.

A simple and practically useful model is proposed in this paper, which depends only on the ambient temperature and relative humidity, and works well in the normal relative humidity and ambient temperature ranges. In Sect. 2 the modeling approach used is introduced. In Sect. 3, the method of evaluating the model parameters is described. In Sect. 4, the sensor responses are modeled using the parameters evaluated by different methods and are compared with those extracted from the datasheets. In Sect. 4, the implications of the model are also discussed with a proposal of a model with fixed parameters for some gas sensors, and finally, in Sect. 5, conclusions are provided.

2. Modeling Approach

The response of a metal oxide chemiresistive gas sensor is generally defined as the ratio of the resistance of the gas sensor in the target gas (R_S) to that in pure air (R_0) or the reciprocal of this ratio.[4] As per Sakai *et al.*, the sensor response is defined as[24]

$$\frac{R_a}{R_g} = 1 + \frac{a_0 C_{A,s}}{AL} T^{-1/4} \exp\left(-\frac{2E_a - E_k}{2RT}\right) \times \tanh\left(ALT^{-\frac{1}{4}} \exp\left(-\frac{E_k}{2RT}\right)\right), \tag{4}$$

where a_0 is the sensitivity coefficient at the reference temperature, $C_{A,s}$ is the concentration of the target at the surface of the sensor material, L is the thickness of the sensing layer, A is a

constant, T is the temperature in ℃, E_a and E_k are activation energies of transduction and diffusion processes on the surface of the metal oxide sensing layer, respectively, and R is the universal gas constant.

Ghosh and Majumder modified the expression in Eq. (4) as follows and verified it experimentally.[25]

$$\frac{\left|R_a - R_g\right|}{R_a} = \frac{a_0}{6}\exp\left(-\frac{E_a}{2RT}\right)\left(6 + nm_0^2\exp\left(-\frac{E_k}{2RT}\right)T^{-0.5}\right)\left(\frac{C_{AS}}{\cosh\left(m_0\exp\left(-\frac{E_k}{2RT}\right)T^{-0.25}\right)}\right)^n \quad (5)$$

Here, n is a constant with a value between 0.6 and 1, and m_0 is a constant depending on the molecular weight of the target gas, pore radius, and sensor layer thickness.

Sakai *et al.* also reported that in the temperature range of 200 to 400 ℃, which is the normal operating temperature range of commercial metal oxide gas sensors, $\frac{R_a}{R_g}$ is proportional to $1 + a_0 C_{A,s}\exp\left(-\frac{E_a}{RT}\right)$.[24] Thus, the sensor response shows an exponential relationship to the temperature. Llobet and coworkers. reported that the sensor response vs target gas concentration characteristics follow the Freundlich adsorption isotherm and show an exponential relationship to temperature as shown below.[26,27]

$$G_s = G_{0T}\exp\left(-\frac{E_A}{2RT}\right) + k_T\ \exp\left(-\frac{E_A}{2RT}\right)C^r \quad (6)$$

Here, G_S is the conductance of the sensing layer when the target gas concentration is C, G_{0T} is the baseline conductance of the sensing layer in air at the reference temperature, r is a power-law exponent, and k_T is the pre-exponential factor at the reference temperature. E_A is the activation energy of target gases for a change in conductance.

For commercial metal oxide sensors, the thickness of the sensing layer, pore radius on the surface of the sensing layer, activation energies, and so forth. can be assumed to be fixed. Therefore, the resistance at the reference temperature and relative humidity is taken as a constant (R_{S0}).

Ménini *et al.* investigated metal oxide gas sensors with and without dopants and observed that they behave very differently at very low relative humidities (below 25%).[28] Samad *et al.* reported that the effect of relative humidity is generally compensated by subtracting a humidity factor from the sensor response.[29] Therefore, we propose a model for calculating the dependence of the sensor response of metal oxide gas sensors on ambient temperature and relative humidity, as follows.

$$\frac{R_S}{R_{S0}} = m_{RH} + \exp\left(g_T\frac{\left(T_c - T_a\right)}{T_c}\right) \quad (7)$$

Here, T_C is the center temperature (reference temperature) in kelvin, T_a is the ambient temperature in kelvin, R_S is the resistance of the metal oxide gas sensor at a particular concentration of the target gas, R_{S0} is the resistance of the metal oxide gas sensor at the reference humidity, center temperature, and the specific value of target gas concentration, g_T is the coefficient of ambient temperature dependence (temperature coefficient in short), and m_{RH} is the humidity factor.

Delpha *et al.* reported that the resistance of TGS832, a metal oxide gas sensor, is proportional to the sum of exponentials of humidity ratios.[30] However, in all the commercially available sensors, we have observed that the sensor response vs temperature characteristics at different relative humidities are plots of the same shape with a constant vertical shift. On further analysis, we have seen that the humidity factor follows a linear relationship to the relative humidity, as follows.

$$m_{RH} = m_{RH_0} + h_{RH}\left(RH - RH_0\right) \tag{8}$$

Here, RH is the relative humidity at which m_{RH} is calculated, RH_0 is the reference relative humidity, h_{RH} is the coefficient of relative humidity dependence of the gas sensor, and m_{RH_0} is the correction factor.

3. Evaluation of Model Parameters

3.1 Extraction of sensor response

The sensor response vs temperature characteristics at various relative humidities are extracted from the datasheets of Zhengzhou Winsen MQ series gas sensors.[31–35] In the datasheets of MQ series gas sensors, the sensor response is provided for a temperature range from −10 to 50 °C at two or three RH values. In most cases, the sensor response is extracted from the plots at an interval of 5 °C. In some cases, where the temperature range is very small, the interval is also made small to have enough values to evaluate the model parameters.

3.2 Evaluation of temperature coefficient and humidity factor

At the reference humidity and center temperature, the sensor response has a numerical value of one, or, in other words, $R_S = R_{S0}$. As a first step, we have taken the humidity factor at the reference humidity (m_{RH}) as zero and calculated the temperature coefficient, from Eq. (7), as

$$g_T = \frac{T_c}{\left(T_c - T_a\right)} \ln\left(\frac{R_s}{R_{s0}}\right). \tag{9}$$

The temperature coefficient is not evaluated at temperatures very close to the center

temperature. Thus, if there are p entries, in the dataset obtained from the sensor response vs temperature characteristics excluding the center temperature, there will be p values for the temperature coefficient. Then, a temperature coefficient set is formed for optimizing the temperature coefficient. The minimum of this set is the minimum of the p-value dataset. In the same way, the maximum of this set is the maximum of the p-value dataset. All minimum to maximum values with an increment of 1.0×10^{-2} are included in the new dataset. The sensor response is calculated by substituting each temperature coefficient in Eq. (7) and by taking m_{RH} as equal to zero. The temperature coefficient that gives a minimum RMS error, when the calculated sensor response is compared with the extracted sensor response, is taken as the optimum temperature coefficient.

All the calculations were conducted after converting the temperatures from °C to K. Sensor response vs temperature characteristics, in the datasheets at different RH values, are of the same shape with a constant vertical shift. Therefore, the humidity factor (m_{RH}) is treated as independent of temperature. Thus, m_{RH} is calculated using Eq. (8) from the difference between the sensor response extracted from the datasheet at a particular RH value and that calculated at the reference humidity. The average of the sensor response differences, at all temperatures, is taken as the optimum value of the humidity factor. The humidity factor calculated at the reference humidity is taken as a correction factor, m_{RH0}. m_{RH0} is evaluated as the average of the calculated [from Eq. (7) taking $m_{RH} = 0$] and extracted sensor response differences at various temperatures at the reference humidity.

3.3 Evaluation of humidity coefficient

The humidity coefficient is calculated using Eq. (8) as

$$h_{RH} = \frac{m_{RH} - m_{RH_0}}{RH - RH_0}. \tag{10}$$

The humidity coefficient is calculated at different RH values, other than the reference humidity, provided in the datasheet. When there is more than one RH value, other than the reference humidity, the evaluated humidity coefficients show a small difference. In such cases, the average humidity coefficient is calculated to have a constant value for each sensor. Instead of using Eq. (10), we have also tried to optimize the humidity coefficient evaluated using Eq. (7) as follows.

$$h_{RH} = \frac{\left(S - m_{RH_0} - \exp\left(g_T \frac{\left(T_c - T_a \right)}{T_c} \right) \right)}{RH - RH_0} \tag{11}$$

Here, S is the extracted sensor response at ambient temperature T_a and relative humidity RH. The humidity coefficient is not calculated at the reference humidity or near the center temperature.

From the range of values obtained, the humidity coefficient that gives the minimum RMS error is selected as the optimum value. A constant humidity coefficient is obtained for each sensor by taking the average of humidity coefficients obtained at various RH values. This value is approximated to a multi-sensor constant wherever the humidity coefficients are nearly equal. In all the methods of calculating the humidity coefficient, the RMS error is calculated by comparing the calculated and extracted sensor responses.

The sensor responses at various ambient temperatures and relative humidities are calculated using Eqs. (7) and (8) after finding out the optimum values of the temperature coefficient, humidity coefficient, and correction factor. The calculated and extracted sensor responses are plotted for the temperature and relative humidity ranges in which the sensor response was extracted.

3.4 Experimental setup for the measurement of effects of ambient temperature and relative humidity

Figure 1(a) shows the schematic diagram of the experimental setup for the measurement of the effects of ambient temperature and relative humidity. The experimental setup uses the MQ series gas sensors produced by Zhengzhou Winsen Electronics Technologies Co., Ltd. The MQ gas sensor modules consist of a load resistor connected in series with the gas sensor to act like a potential divider when the power is applied. The supply voltage is +5 V. The voltage across the load resistor with respect to the ground is taken as the analog output. DHT11 produced by Guangzhou Aosong Electronics Co., Ltd. is used for sensing the ambient temperature and relative humidity. DHT11 provides a serial output that contains the integer and fractional values of the measured temperature and relative humidity. NodeMCU version 1.0 developed by Espressif Systems, which is a microcontroller with a built-in WiFi module, was used for data collection and transmission. Since the number of pins is limited, we used ZADCS147, which is a

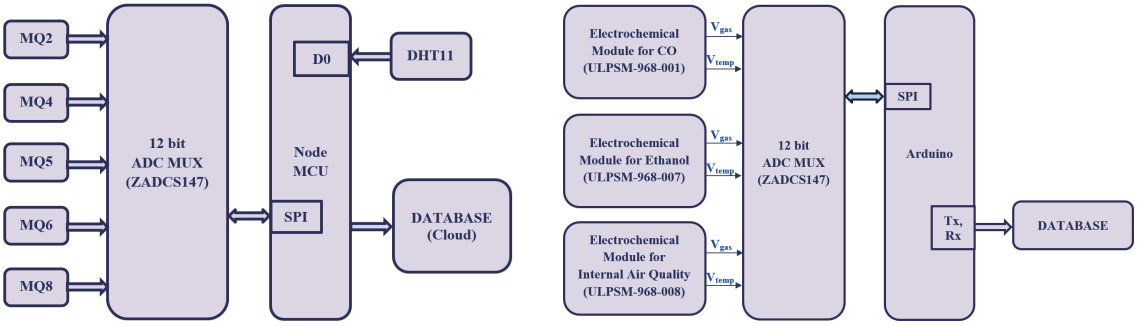

Fig. 1. (Color online) Schematic diagram of the experimental setup for measurement of the effects of ambient temperature and relative humidity. (a) Setup to measure the resistance of MQ series sensors, ambient temperature, and relative humidity, and (b) test setup with electrochemical (SPEC) sensors to measure the target gas concentration in the atmosphere.

12-bit 8-channel ADC MUX produced by Zentrum Mikroelektronik Dresden (ZMDI) Germany, to connect MQ series gas sensors to NodeMCU. ZADCS147 converts the analog voltage output from the five MQ series gas sensors into digital and sends it to NodeMCU serially through a serial peripheral interface (SPI).

All the collected data are sent to a cloud database through WiFi using NodeMCU. Herzner Virtual Private Server (VPS) is the cloud server used for this work. This cloud server is configured as a Platform as a service (PaaS). CapRover is used for server management. Three docker containers are created in the server. In the first container, a certificate-based client authentication mosquito MQTT broker is written and installed. In the second docker container, a PAHO Python client is created and installed as the MQTT client for subscribing the published sensor data from the sensor node to the MQTT broker in a specific topic. The third docker container is used for the database. MySQL is used to store the sensor data tables.

Figure 1(b) shows the schematic diagram of the test setup with precalibrated electrochemical sensor modules produced by SPEC Sensors LLC. These ultralow-power sensor modules (ULPSMs) are used for measuring the real concentration of gases to which the MQ series gas sensors that we used have high sensitivity. Since precalibrated electrochemical sensors are used, they have high sensitivity even at a very low concentration of target gases and have good accuracy. The MQ series gas sensors under consideration are MQ2, MQ4, MQ5, MQ6, and MQ8. These sensors have high sensitivity to gases such as CO, CH_4, ethanol, and H_2. The electrochemical sensor modules used in the test setup are ULPSM-CO-968-001, ULPSM-IAQ-968-007, and ULPSM-ETOH-968-007. These sensors are sensitive to gases such as CO, ethanol, H_2S, SO_2, and NO. The calibration details of the electrochemical sensors used in the ULPSM boards are provided as a QR code on the sensor. The ULPSM boards have two analog outputs, V_{gas} and V_{temp}. These voltages correspond to the target gas concentration and ambient temperature. The signals from the three electrochemical sensor boards are fed to the Arduino Uno R3 board using the ZADCS147 ADCMUX. The data collected are stored in a local personal computer (PC) and sent from the Arduino through the serial port of the PC. The concentration can be calculated using V_{gas} and the parameters given in the calibration data using the method given in the datasheets of ultralow-power sensor modules. The GX-2009 produced by Riken Keiki Instruments, which is a portable multi-gas detector, is used for confirming that the concentrations of H_2 and CH_4 are zero when the resistance in pure air is measured.

3.5 Measurement and correction of the effects of ambient temperature and relative humidity

The experimental setup with MQ series sensors is placed at three locations in and around our campus along with the test setup, for a total duration of four months. The T_a and RH value, and the resistances of MQ series sensors are stored in the database at an interval of 10 min. The accurate target gas concentration is obtained from the test setup with electrochemical sensors and the portable multi-gas detector. The concentrations of all target gases are assumed to be zero

when the target gas concentration, measured with the test setup, is below 5% of the minimum detectable value of MQ series sensors. In these situations when the gas sensors are assumed to be insensitive to the target gases, the resistance obtained from the MQ series sensors is selected as resistance in pure air. In the instances when the target gas concentration is almost zero, the effects of T_a and RH are calculated using Eqs. (7) and (8). Then, the resistance in air at the reference humidity and center temperature is calculated by compensating for the effects of T_a and RH. The resistance in air of each gas sensors, after compensation, are plotted along with the resistance in air without compensation against various values of ambient temperature at different relative humidity. The deviations in resistance from its average value, with and without compensation, are studied.

4. Results and Discussions

4.1 Extraction of model parameters and comparison of sensor responses

Table 1 gives the model parameter value of MQ series gas sensors and the RMS error of the calculated sensor response with the sensor response extracted from the datasheet. Figures 2(a)–2(e) show the calculated and extracted sensor responses of MQ series gas sensors. For MQ4, MQ5, and MQ6, the reference humidity and center temperature are selected as 33% and 20 °C, respectively. For MQ2 and MQ8, the reference humidity and center temperature are selected as 60% and 25 °C, respectively.

Figure 2(a) shows the sensor response vs temperature characteristics of the MQ4 gas sensor at RH values of 33 and 85% with the sensor response calculated using the model proposed. At the RH value of 33%, when T_a ranges from −10 to 50 °C, the sensor response varies from 1.28 to 0.90. The temperature coefficient and humidity factor are 1.78 and 2.91×10^{-2}, respectively, and the model proposed predicts the sensor response with an RMS error of 2.99×10^{-2}. The maximum deviation in sensor response is 4.90×10^{-2} at –10 °C. At the RH value of 85%, when T_a ranges from −10 to 50 °C, the sensor response varies from 1.09 to 0.73. The temperature coefficient and humidity factor are 1.78 and -13.21×10^{-2}, respectively, and the model proposed

Table 1
Calculated temperature coefficients and humidity factors of MQ series gas sensors at various relative humidities.

Sensor	*RH* (%)	g_T	m_{RH}	RMS Error
MQ4	33	1.78	2.91×10^{-2}	2.99×10^{-2}
	85		-13.21×10^{-2}	1.58×10^{-2}
MQ5	33	2.35	1.68×10^{-2}	4.04×10^{-2}
	85		-14.79×10^{-2}	3.55×10^{-2}
MQ6	33	1.95	3.47×10^{-2}	3.68×10^{-2}
	85		-11.88×10^{-2}	3.47×10^{-2}
MQ2	30	3.30	19.41×10^{-2}	4.67×10^{-2}
	60		0.39×10^{-2}	2.20×10^{-2}
	85		-13.74×10^{-2}	3.65×10^{-2}
MQ8	30	3.31	20.01×10^{-2}	4.50×10^{-2}
	60		0.73×10^{-2}	2.30×10^{-2}
	85		-13.40×10^{-2}	3.85×10^{-2}

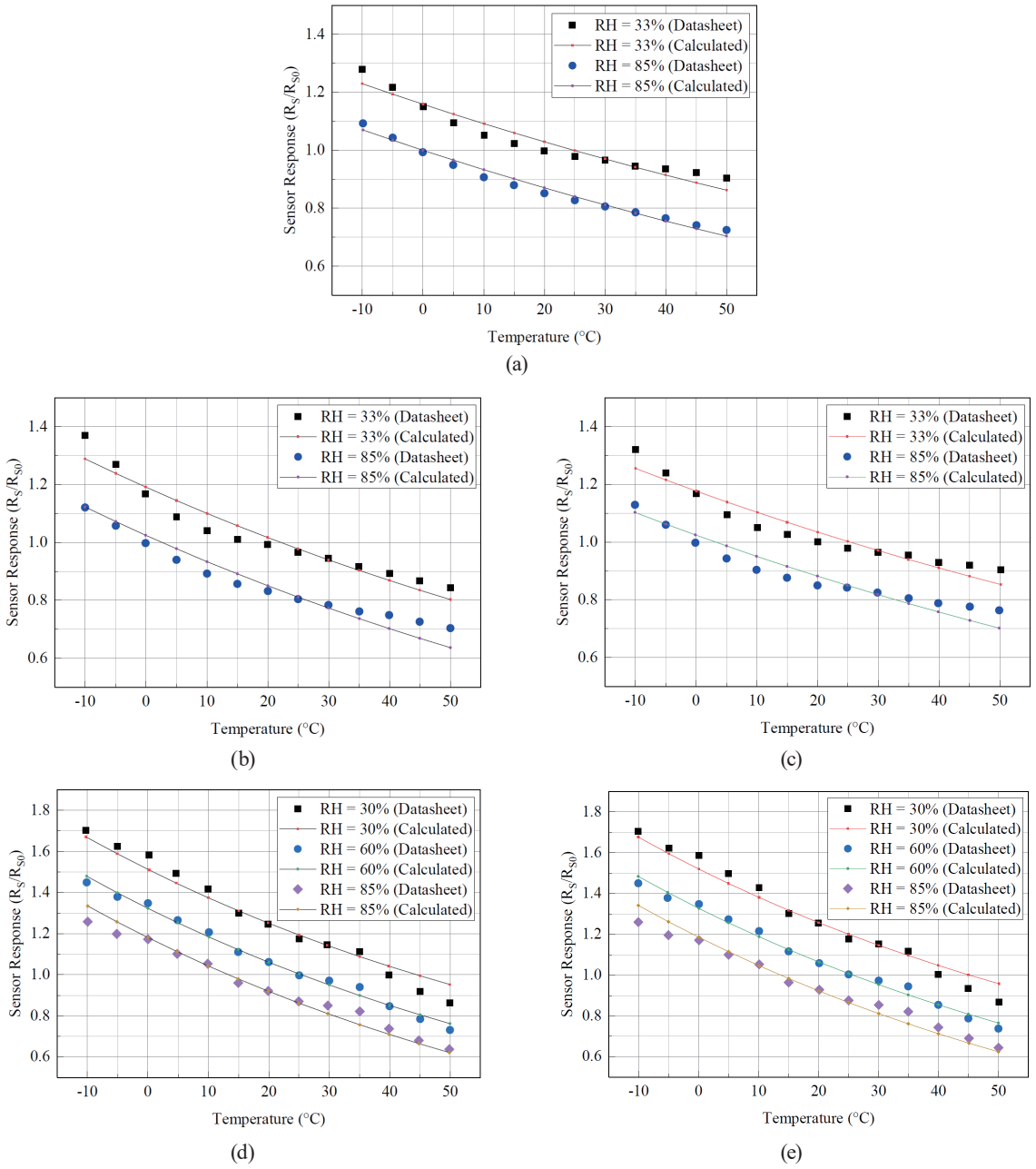

Fig. 2. (Color online) Comparison of sensor response extracted from data sheets of MQ series gas sensors with that calculated using model parameters: (a) MQ4 at 1000 ppm methane, (b) MQ5 at 1000 ppm hydrogen, (c) MQ6 at 1000 ppm LPG, (d) MQ2 at 1000 ppm butane, and (e) MQ8 at 1000 ppm hydrogen.

predicts the sensor response with an RMS error of 1.58×10^{-2}. The maximum deviation is 2.63×10^{-2} at 10 °C.

Figure 2(b) shows the sensor response vs temperature characteristics of the MQ5 gas sensor at RH values of 33 and 85% with the sensor response calculated using the model proposed. At the RH value of 33%, when T_a ranges from −10 to 50 °C, the sensor response varies from 1.37 to

0.84. The temperature coefficient and humidity factor are 2.35 and 1.68×10^{-2}, respectively, and the model proposed predicts the sensor response with an RMS error of 4.04×10^{-2}. The maximum deviation in sensor response is 8.04×10^{-2} at –10 °C. At the RH value of 85%, when T_a ranges from −10 to 50 °C, the sensor response varies from 1.12 to 0.70. The temperature coefficient and humidity factor are 2.35 and -14.79×10^{-2}, respectively, and the model proposed predicts the sensor response with an RMS error of -3.55×10^{-2}. The maximum deviation in sensor response is 6.71×10^{-2} at 50 °C.

Figure 2(c) shows the sensor response vs temperature characteristics of the MQ6 gas sensor at RH values of 33 and 85% with the sensor response calculated using the model proposed. At the RH value of 33%, when T_a ranges from −10 to 50 °C, the sensor response varies from 1.32 to 0.90. The temperature coefficient and humidity factor are 1.95 and 3.47×10^{-2}, respectively, and the model proposed predicts the sensor response with an RMS error of 3.68×10^{-2}. The maximum deviation in sensor response is 6.55×10^{-2} at –10 °C. At the RH value of 85%, when T_a ranges from −10 to 50 °C, the sensor response varies from 1.13 to 0.76. The temperature coefficient and humidity factor are 1.95 and -11.88×10^{-2}, respectively, and the model proposed predicts the sensor response with an RMS error of 3.47×10^{-2}. The maximum deviation in sensor response is 6.19×10^{-2} at 50 °C.

Figure 2(d) shows the sensor response vs temperature characteristics of the MQ2 gas sensor at RH values of 30, 60, and 85% with the sensor response calculated using the model proposed. At the RH value of 30%, when T_a ranges from −10 to 50 °C, the sensor response varies from 1.70 to 0.86. The temperature coefficient and humidity factor are 3.30 and 19.41×10^{-2}, respectively, and the model proposed predicts the sensor response with an RMS error of 4.67×10^{-2}. The maximum deviation in sensor response is 8.84×10^{-2} at 50 °C. At the RH value of 60%, when T_a ranges from −10 to 50 °C, the sensor response varies from 1.45 to 0.73. The temperature coefficient and humidity factor are 3.30 and 0.39×10^{-2}, respectively, and the model proposed predicts the sensor response with an RMS error of 2.20×10^{-2}. The maximum deviation in sensor response is 4.13×10^{-2} at 35 °C. At the RH value of 85%, when T_a ranges from −10 to 50 °C, the sensor response varies from 1.26 to 0.64. The temperature coefficient and humidity factor are 3.30 and -13.74×10^{-2}, respectively, and the model proposed predicts the sensor response with an RMS error of 3.65×10^{-2}. The maximum deviation in sensor response is 7.72×10^{-2} at –10 °C.

Figure 2(e) shows the sensor response vs temperature characteristics of the MQ8 gas sensor at RH values of 30, 60, and 85% with the sensor response calculated using the model proposed. At the RH value of 30%, when T_a ranges from −10 to 50 °C, the sensor response varies from 1.70 to 0.87. The temperature coefficient and humidity factor are 3.31 and 20.01×10^{-2}, respectively, and the model proposed predicts the sensor response with an RMS error of 4.50×10^{-2}. The maximum deviation in sensor response is 8.90×10^{-2} at 50 °C. At the RH value of 60%, when T_a ranges from −10 to 50 °C, the sensor response varies from 1.45 to 0.74. The temperature coefficient and humidity factor are 3.31 and 0.73×10^{-2}, respectively, and the model proposed predicts the sensor response with an RMS error of 2.30×10^{-2}. The maximum deviation in sensor response is 4.18×10^{-2} at 35 °C. At the RH value of 85%, when T_a ranges from −10 to 50 °C, the sensor response varies from 1.26 to 0.63. The temperature coefficient and humidity

factor are 3.31 and -13.40×10^{-2}, respectively, and the model predicts the sensor response with an RMS error of 3.85×10^{-2}. The maximum deviation in sensor response is 8.21×10^{-2} at –10 °C.

Table 1 gives the temperature coefficients and humidity factors along with RMS error, and Table 2 gives the humidity coefficients obtained using various methods and the RMS error in each case. We have approximated the h_{RH} values for similar sensors as multi-sensor humidity coefficients, and the calculated RMS error is also shown in Table 2. For the MQ4 gas sensor, the humidity coefficient is -3.05×10^{-3} at the RH of 85%. The multi-sensor humidity coefficient obtained is -3×10^{-3}. The RMS error changes from 1.60×10^{-2} to 1.66×10^{-2} in the case of RH = 85% when the humidity coefficient is reduced to a single constant for multiple sensors. For the MQ5 gas sensor, the humidity coefficient is -3.20×10^{-3} at the RH of 85%. The multi-sensor humidity coefficient obtained is -3×10^{-3}. The RMS error changes from 3.56×10^{-2} to 3.66×10^{-2} in the case of RH = 85% when the humidity coefficient is reduced to a single constant for multiple sensors. For the MQ6 gas sensor, the humidity coefficient is -2.94×10^{-3} at the RH of 85%. The multi-sensor humidity coefficient obtained is -3×10^{-3}. The RMS error changes from 3.47×10^{-2} to 3.48×10^{-2} in the case of RH = 85% when the humidity coefficient is reduced to a single constant for multiple sensors.

For the MQ2 gas sensor, the humidity coefficients are -6.32×10^{-3} and -5.68×10^{-3} at RH values of 30 and 85%, respectively. The multi-sensor humidity coefficient obtained is -6×10^{-3}. The RMS error changes from 4.67×10^{-2} to 4.78×10^{-2} in the case of RH = 30% and from 3.65×10^{-2} to 3.75×10^{-2} in the case of RH = 85% when the humidity coefficient is reduced to a single constant for multiple devices. For the MQ8 gas sensor, the humidity coefficients are -6.43×10^{-3} and -5.66×10^{-3} at RH values of 30 and 85%, respectively. The multi-sensor humidity coefficient obtained is -6×10^{-3}. The RMS error changes from 4.50×10^{-2} to 4.68×10^{-2} in the case of RH = 30% and from 3.85×10^{-2} to 3.95×10^{-2} in the case of RH = 85% when the humidity coefficient is reduced to a single constant for multiple sensors.

In Table 1, the temperature coefficients of the MQ2 and MQ8 gas sensors are reported as 3.30 and 3.31, respectively. From Table 2, the multi-sensor humidity coefficient is -6×10^{-3} for the MQ2 and MQ8 gas sensors. If the temperature coefficient is approximated to 3.3, the model with

Table 2
Humidity coefficients evaluated using various methods at relative humidity other than the reference value and the RMS error in sensor response for the respective cases.

Sensor	RH (%)	h_{RH} calculated using Eq. (11)		$h_{RH} = \frac{m_{RH} - m_{RH_0}}{RH - RH_0}$		h_{RH} approximated to a single value for multiple sensors	
		h_{RH}	RMS Error	h_{RH}	RMS Error	h_{RH}	RMS Error
MQ4	85	-3.05×10^{-3}	1.60×10^{-2}	-3.10×10^{-3}	1.58×10^{-2}	-3×10^{-3}	1.66×10^{-2}
MQ5	85	-3.20×10^{-3}	3.56×10^{-2}	-3.17×10^{-3}	3.55×10^{-2}	-3×10^{-3}	3.66×10^{-2}
MQ6	85	-2.94×10^{-3}	3.47×10^{-2}	-2.95×10^{-3}	3.47×10^{-2}	-3×10^{-3}	3.48×10^{-2}
MQ2	30	-6.32×10^{-3}	4.67×10^{-2}	-6.34×10^{-3}	4.67×10^{-2}	-6×10^{-3}	4.78×10^{-2}
	85	-5.68×10^{-3}	3.65×10^{-2}	-5.65×10^{-3}	3.65×10^{-2}	-6×10^{-3}	3.75×10^{-2}
MQ8	30	-6.43×10^{-3}	4.50×10^{-2}	-6.43×10^{-3}	4.50×10^{-2}	-6×10^{-3}	4.68×10^{-2}
	85	-5.66×10^{-3}	3.85×10^{-2}	-5.65×10^{-3}	3.85×10^{-2}	-6×10^{-3}	3.95×10^{-2}

the same model parameters can be used for the MQ2 and MQ8 gas sensors for all practical purposes. In the case of the MQ4, MQ5, and MQ6 gas sensors, the temperature coefficients are 1.78, 2.35, and 1.95, respectively, but the multi-sensor humidity coefficient is -3×10^{-3}. From Table 2, even in the case of a single-value multi-sensor humidity coefficient, in MQ series sensors, the RMS error is less than 5% of the sensor response range for all the sensors analyzed. Therefore, we can use the multi-sensor humidity coefficient given in Table 2 for all practical purposes.

From Figs. 2(a)–2(e), it is evident that the maximum error in the calculated and extracted sensor responses is less than 10% of its datasheet value all the time. The sensor response calculated using the model shows larger deviations at relative humidity values near 33 and 85%, which means either extremity of the humidity range. These deviations are higher at a temperature above 40 °C. The characteristics have some deviation in the region of 0 to 20 °C, but it is around 5% of the datasheet values. As per Yamazoe and Simanoe, and Llobet *et al.*, the resistance of the metal oxide gas sensor is proportional to C^n,[9,26] where C is the concentration of the target gas and n is the power law exponent with a value near 0.5 when detecting reducing gases. Thus, a deviation less than 10% in the temperature dependence curve will not cause an error of more than 5% in the target gas concentration measurement. Our model may need a correction with higher order terms of temperature and humidity to hold with the datasheet values at a temperature above 40 °C. This increases the computational complexity by a large amount. Adding such a correction is not necessary for the MQ series gas sensors as the benefit is less than the huge complexity added.

4.2 Measurement of the resistance in pure air and compensation of effects of ambient temperature and relative humidity

Figures 3(a)–3(e) show the comparison of resistances of MQ series gas sensors in pure air with and without the compensation of the effects of ambient temperature and relative humidity at selected RH and T_a values. The resistance in pure air at the same temperature and RH measured with the same MQ series sensor at different instances showed a slight variation. The average of the measured resistances is used in such cases. When the concentration of the target gases was assumed to be zero, the resistance was measured at RH values of 65, 70, 75, 80, and 85%. Figure 3(a) shows the resistance of the MQ4 gas sensor in air, with and without the compensation of the effects of ambient temperature and relative humidity. When T_a ranges from 23 to 33 °C and RH varies from 65 to 85%, the measured resistance in pure air varies from 2.41×10^3 to 3.28×10^3 Ω. After the compensation of the effects of ambient temperature and relative humidity, the resistance in pure air ranges from 4.06×10^3 to 4.20×10^3 Ω with an average of 4.14×10^3 Ω.

Figure 3(b) shows the resistance of the MQ5 gas sensor in air, with and without the compensation of the effects of ambient temperature and relative humidity. When T_a ranges from 23 to 33 °C and RH varies from 65 to 85%, the measured resistance in pure air varies from 1.56×10^4 to 2.22×10^4 Ω. After the compensation of the effects of ambient temperature and relative humidity, the resistance in pure air ranges from 2.74×10^4 to 2.85×10^4 Ω with an average of 2.79×10^4 Ω.

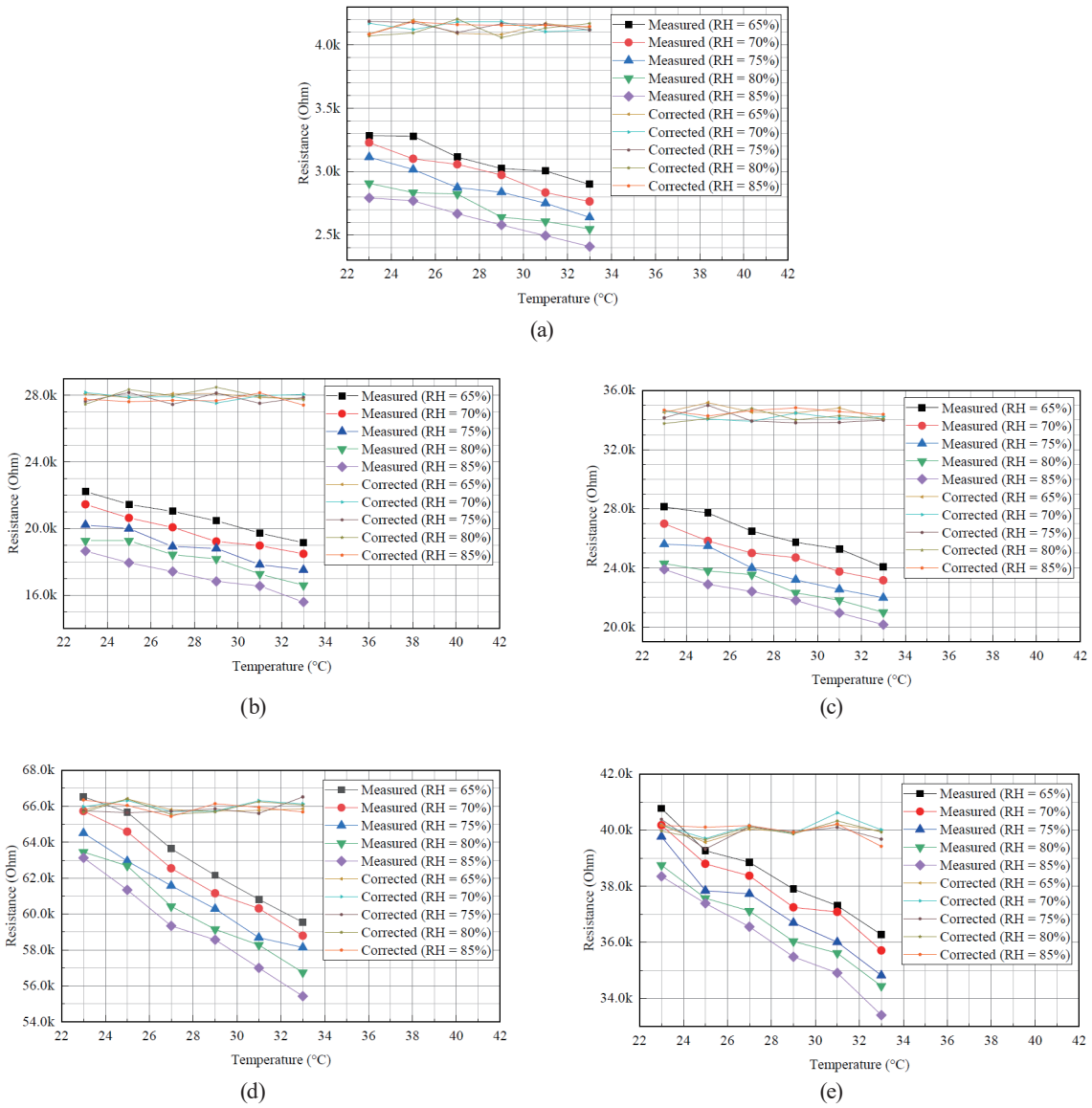

Fig. 3. (Color online) Comparison of resistances of MQ series gas sensors in pure air measured using the experimental setup in Fig. 1. (Color online) (a) With the resistance obtained after compensation of effects of ambient temperature and relative humidity: (a) MQ4, (b) MQ5, (c) MQ6, (d) MQ2, and (e) MQ8.

Figure 3(c) shows the resistance of the MQ6 gas sensor in air, with and without the compensation of the effects of ambient temperature and relative humidity. When T_a ranges from 23 to 33 °C and RH varies from 65 to 85%, the measured resistance in pure air varies from 2.02×10^4 to 2.77×10^4 Ω. After the compensation of the effects of ambient temperature and relative humidity, the resistance in pure air ranges from 3.35×10^4 to 3.52×10^4 Ω with an average of 3.43×10^4 Ω.

Figure 3(d) shows the resistance of the MQ2 gas sensor in air, with and without the compensation of the effects of ambient temperature and relative humidity. When T_a ranges from

23 to 33 °C and RH varies from 65 to 85%, the measured resistance in pure air varies from 5.54×10^4 to 6.65×10^4 Ω. After the compensation of the effects of ambient temperature and relative humidity, the resistance in pure air ranges from 6.54×10^4 to 6.65×10^4 Ω with an average of 6.59×10^4 Ω.

Figure 3(e) shows the resistance of the MQ8 gas sensor in air, with and without the compensation of the effects of ambient temperature and relative humidity. When T_a ranges from 23 to 33 °C and RH varies from 65 to 85%, the measured resistance in pure air varies from 3.34×10^4 to 4.08×10^4 Ω. After the compensation of the effects of ambient temperature and relative humidity, the resistance in pure air ranges from 3.93×10^4 to 4.06×10^4 Ω with an average of 3.99×10^4 Ω.

From Figs. 3(a)–3(e), we can see that when compensation is applied, the resistance in pure air has a less than 3% variation from its average. Without compensation, the variation in resistance in the air is around 20% when RH varies from 60 to 85% and T_a from 23 to 33 °C.

5. Conclusions

In this paper, we have proposed a simple mathematical model, for typical metal oxide chemiresistive gas sensors, to compensate for the effects of temperature and humidity. This model is useful for the end user because it uses only the values that are easily measurable or available. The researchers working in this area may also find it very useful since most of the measurements/models do not consider the effect of humidity and have a measurement error. In the sensors that we have analyzed, the sensor response varies from 60 to 170% (for the same gas concentration in normal ambient temperature and relative humidity range) of the sensor response at the center temperature and reference humidity. The measured resistance in pure air (after the temperature and humidity correction) is within the limit of ±3% of its average. We have observed that even when the humidity coefficient is approximated to one value for similar sensors, the RMS error is less than 5%. The sensor response calculated using the model is a good match with that extracted from datasheets. We have also observed that the same humidity coefficient fits multiple sensors. In MQ2 and MQ8, all the model parameters are observed to be the same.

Acknowledgments

This work was supported by the Rural Technology Development Centre, Government College of Engineering Kannur, Kerala 670563, India.

References

1 A. Dey: Mater. Sci. Eng. B **229** (2018) 206. https://doi.org/10.1016/j.mseb.2017.12.036
2 X. Liu, S. Cheng, H. Liu, S. Hu, D. Zhang, and H. Ning: Sensors **12** (2012) 9635. https://doi.org/10.3390/s120709635
3 A. Gaskov, M. Rumyantseva, and A. Marikutsa: Tin Oxide Materials, M. O. Orlandi, Ed. (Elsevier, Amsterdam, 2020) Chap. 7. https://doi.org/10.1016/B978-0-12-815924-8.00007-4
4 N. Yamazoe and K. Shimanoe: Semiconductor Gas Sensors, R. Jaaniso and O. K. Tan, Eds. (Woodhead Publishing, Cambridge,2020) Chap. 1. https://doi.org/10.1016/B978-0-08-102559-8.00001-X
5 H. Ji, W. Zeng, and Y. Li: Nanoscale **11** (2019) 22664. https://doi.org/10.1039/C9NR07699A

6 J. Savioli, A. L. Gavin, A. K. Lucid, and G. W. Watson: Tin Oxide Materials, M. O. Orlandi, Ed. (Elsevier, Amsterdam, 2020) Chap. 2. https://doi.org/10.1016/B978-0-12-815924-8.00002-5
7 T. Sahm, A. Gurlo, N. Barsan, and U. Weimar: Sens. Actuators, B **118** (2006) 78. https://doi.org/10.1016/j.snb.2006.04.004
8 T. Sahm, A. Gurlo, N. Barsan, U. Weimar, and L. Mädler: Thin Solid Films **490** (2005) 43. https://doi.org/10.1016/j.tsf.2005.04.013
9 N. Yamazoe and K. Shimanoe: J. Sens. **2009** (2009) 1. https://doi.org/10.1155/2009/875704
10 N. Yamazoe and K. Shimanoe: Sens. Actuators, B **160** (2011) 1352. https://doi.org/10.1016/j.snb.2011.09.075
11 P. Shankar and J. B. B. Rayappan: Sci. Lett. J. **4** (2015) 126.
12 A. Fort, M. Mugnaini, S. Rocchi, V. Vignoli, E. Comini, G. Faglia, and A. Ponzoni: Sens. Actuators, B **148** (2010) 283. https://doi.org/10.1016/j.snb.2010.04.034
13 B. Mehrabi Matin, Y. Mortazavi, A. A. Khodadadi, A. Abbasi, and A. Anaraki Firooz: Sens. Actuators, B **151** (2010) 140. https://doi.org/10.1016/j.snb.2010.09.033
14 O. Wurzinger and G. Reinhardt: Sens. Actuators, B **103** (2004) 104. https://doi.org/10.1016/j.snb.2004.04.041
15 M. S. Chavali and M. P. Nikolova: SN Appl. Sci. **1** (2019) 607. https://doi.org/10.1007/s42452-019-0592-3
16 M. Al-Hashem, S. Akbar, and P. Morris: Sens. Actuators, B **301** (2019) 126845. https://doi.org/10.1016/j.snb.2019.126845
17 G. Korotcenkov and B. K. Cho: Sens. Actuators, B **244** (2017) 182. https://doi.org/10.1016/j.snb.2016.12.117
18 J. F. McAleer, P. T. Moseley, J. O. W. Norris, D. E. Williams, and B. C. Tofield: J. Chem. Soc. Faraday Trans. 1: Phys. Chem. Condens. Phases **84** (1988) 441. https://doi.org/10.1039/F19888400441
19 M. V. Nikolic, V. Milovanovic, Z. Z. Vasiljevic, and Z. Stamenkovic: Sensors **20** (2020) 6694. https://doi.org/10.3390/s20226694
20 N. Bârsan, M. Huebner, and U. Weimar: Semiconductor Gas Sensors, R. Jaaniso and O. K. Tan, Eds. (Woodhead Publishing, Cambridge, 2020) Chap. 2. https://doi.org/10.1016/B978-0-08-102559-8.00002-1
21 P. Narkhede, R. Walambe, S. Mandaokar, P. Chandel, K. Kotecha, and G. Ghinea: Appl. Syst. Innov. **4** (2021) 1. https://doi.org/10.3390/asi4010003
22 L. Han, C. Yu, K. Xiao, and X. Zhao: Sensors **19** (2019) 1960. https://doi.org/10.3390/s19091960
23 J. M. Ali, M. A. Hussain, M. O. Tade, and J. Zhang: Expert Syst. Appl. **42** (2015) 5915. https://doi.org/10.1016/j.eswa.2015.03.023
24 G. Sakai, N. Matsunaga, K. Shimanoe, and N. Yamazoe: Sens. Actuators, B **80** (2001) 125. https://doi.org/10.1016/S0925-4005(01)00890-5
25 A. Ghosh and S. B. Majumder: Phys. Chem. Chem. Phys. **19** (2017) 23431. https://doi.org/10.1039/c7cp04241h
26 E. Llobet, X. Vilanova, J. Brezmes, D. Lopez, and X. Correig: Sens. Actuators, B **77** (2001) 275. https://doi.org/10.1016/S0925-4005(01)00710-9
27 E. Llobet, J. Rubio, X. Vilanova, J. Brezmes, X. Correig, J. W. Gardner, and E. L. Hines: Sens. Actuators, B **76** (2001) 419. https://doi.org/10.1016/S0925-4005(01)00650-5
28 P. Ménini, F. Parret, M. Guerrero, K. Soulantica, L. Erades, A. Maisonnat, and B. Chaudret: Sens. Actuators, B **103** (2004) 111. https://doi.org/10.1016/j.snb.2004.04.103
29 A. Samad, D. R. Obando Nuñez, G. C. Solis Castillo, B. Laquai, and U. Vogt: Sensors **20** (2020) 5175. https://doi.org/10.3390/s20185175
30 C. Delpha, M. Siadat, and M. Lumbreras: Chem. Microsens. Appl. **3539** (1998) 172. https://doi.org/10.1117/12.333746
31 Technical Datasheet MQ-2 Gas Sensor: https://www.pololu.com/file/0J309/MQ2.pdf (accessed April 2021).
32 Technical Datasheet MQ-4 Gas Sensor: https://www.pololu.com/file/0J311/MQ4.pdf (accessed April 2021).
33 Technical Datasheet MQ-5 Gas Sensor: https://www.winsen-sensor.com/d/files/MQ-5.pdf (accessed April 2021).
34 Technical Datasheet MQ-6 Gas Sensor: https://www.winsen-sensor.com/d/files/semiconductor/mq-6.pdf (accessed April 2021).
35 Technical Datasheet MQ-8 Gas Sensor: hhttps://www.winsen-sensor.com/d/files/semiconductor/mq-8.pdf (accessed April 2021).

About the Authors

K. Sukhdev received his B.Tech. degree in electronics and communication engineering from Kannur University, Government College of Engineering Kannur, Kerala, India, in 2004, and his M.Tech. degree in electronics from Cochin University of Science and Technology, Kerala, India, in 2008. He is currently pursuing his Ph.D. degree in electronics engineering from APJ Abdul Kalam Technological University Kerala, Government College of Engineering Kannur, Kerala, India. He was a lecturer at the Government Polytechnic College Thrikaripur, Kerala, India from 2012 to 2018. He is currently a lecturer in the electronics and communication engineering department, Government Residential Women's Polytechnic College Payyannur, Kerala, India. His research interests include modeling gas sensors and IoT networks.

P. Harinarayanan received his B.Tech. degree in electronics and communication engineering from Kannur University, Government College of Engineering Kannur, Kerala, India, in 2004, and his M.Tech. degree in signal processing and embedded systems from APJ Abdul Kalam Technological University Kerala, Government College of Engineering Kannur, Kerala, India in 2021. He is currently a lecturer in the electronics and communication engineering department, Government Residential Women's Polytechnic College Payyannur, Kerala, India. His research interests include air quality, embedded communication systems, and IoT networks.

U. Sajesh Kumar received his B.Tech. degree in electronics and communication engineering from Calicut University, Government College of Engineering Thrissur, Kerala, India, in 2001, his M.Tech. degree in microelectronics and VLSI from the National Institute of Technology Calicut, Kerala, India, in 2010, and his Ph.D. degree in nanoelectronics from the Indian Institute of Technology Bombay, Maharashtra, India, in 2017. He is currently an associate professor in the electronics and communication engineering department, Government College of Engineering Kannur, Kerala, India. His research interests include nanoelectronics, MEMS, and IoT networks.

P. Baburaj received his B.Tech. degree in electrical and electronics engineering from Calicut University, Government College of Engineering Kannur, Kerala, India, in 1995, his M.Tech. degree in signal processing from the Indian Institute of Technology Guwahati, Assam, India, in 2007, and his Ph.D. degree in control of data transmission networks from the Indian Institute of Technology Bombay, Maharashtra, India, in 2015. He is currently an associate professor in the electrical and electronics engineering department, Government College of Engineering Kannur, Kerala, India. His research interests include control of data transmission networks and IoT networks.